Journal of Thermal Science Vol.31, No.3 (2022) 816−829

https://doi.org/10.1007/s11630-022-1586-9 **Article ID: 1003-2169(2022)03-0816-14**

Experimental Investigation on Pouch Lithium-ion Battery Thermal Management with Mini-Channels Cooling Plate Based on Heat Generation Characteristic

REN Honglei[1], JIA Li[1*], DANG Chao[1*], YANG Chengliang[1], JIA Hongyang[2], LIU Junjie[2]

1. Beijing Key Laboratory of Flow and Heat Transfer of Phase Changing in Micro and Small Scale, School of Mechanical, Electronic and Control Engineering, Beijing Jiaotong University, Beijing 100044, China
2. CRRC Dalian Institute Co., LTD., Dalian 116021, China

Abstract: An electrochemical thermal coupling model of lithium battery was established to study the heat generation characteristic in this study. The simulation results showed that the heat generation density of the battery increased with the discharge rate. With the discharge process, the heat generation density of the battery increased continuously. With 2.5C discharge rate, the heat generation density at the end of discharge was 1.82 times of that at the beginning of discharge. The heat generation density at different areas of the battery was not uniform and 46% of the total ohmic heat was generated near the electrode tabs. A cooling plate with variable mini-channels was designed to improve the temperature non-uniformity caused by the heat generation characteristic. A cooling plate with uniform mini-channels was designed for compared experiment. The experiments were conducted with deionized water and refrigerant R141b and carried out with 1.5C, 2C and 2.5C discharge rates. Experimental results showed that the cooling plate with variable mini-channels had a better cooling performance in both single-phase and two-phase cooling conditions.

Keywords: lithium-ion battery, mini-channels cooling plate, heat generation characteristic, thermal management

1. Introduction

In recent years, Electric Vehicles (EVs) have become popular over the world due to their high energy efficiency and large potential to reduce the emission of fossil fuel combustion pollutants in urban areas. From the perspective of solving the utilization of renewable energy (photovoltaic power generation, wind power generation, etc.), reducing pollutant emissions in densely populated areas, and alleviating the pressure of environmental pollution in large cities, electric vehicles are the main direction for the development of the transportation industry in the future. As the main energy storage component of EVs, lithium-ion battery has drawn the intensive attention of researchers.

As a type of power lithium-ion battery, pouch lithium-ion battery has been developed in EVs recently. But the safety, cycle-life and performance of lithium-ion battery are very sensitive to its working temperature [1]. There are two kinds of temperature problems: the battery temperature may exceed the allowable temperature range because of heat generation in the batteries, leading to

Received: Apr 01, 2021
AE: LI Yinshi
Corresponding author: JIA Li; E-mail: ljia@bjtu.edu.cn
DANG Chao Dangchao@bjtu.edu.cn

Nomenclature

c_l	Li^+ concentration in liquid phase/mol·m^{-3}
F	Faraday constant, 96 485 C·mol^{-1}
i	current density/A
i_{app}	applied current density/A·m^{-2}
j_{loc}	local current density/A·m^{-2}
L_{neg}	thickness of negative electrode/ m
L_{pos}	thickness of positive electrode/μm
L_{sep}	thickness of separator/μm
N_l	liquid ion flux/A·m^{-2}
Q_{act}	active heat generation/J
Q_{ave}	average heat generation density/J
Q_{cc}	heat generation of current collectors/J
Q_{ohm}	Ohmic heat generation/J
Q_{rea}	reaction heat generation/J
Q_{total}	total heat generation/J
S	entropy/J·mol^{-1}·K^{-1}
S_a	specific surface area/m^{-1}
T	temperature/°C
U_i	open circuit potential/V

Greek letters

δ_{cc}	thickness of current collector/μm
η	over potential/V
σ_l	electric conductivity for liquid phase/S·m^{-1}
σ_s	electric conductivity for solid phase/S·m^{-1}
φ	potential/V

Subscripts and superscripts

0	initial state
act	active heat
cc	current collector
i	neg/negcc/pos/poscc
l	liquid phase
neg	negative electrode
ohm	Ohmic
pos	positive electrode
rea	reaction heat
s	solid phase
sep	separator

dangerous accidents at high discharge rate; the other problem is the temperature uniformity on the internal battery and battery pack. When many cells in a compact module work at different temperatures, each cell is charged and discharged differently during every charge and discharge cycle, and it will bring about some difference in the state of charge between different cells. This would be amplified for large difference with the long time operation [2]. Effective thermal management for lithium-ion battery module is an indispensable part to guarantee the operating safety, extending the cycle-life and improving the operating performance of batteries. Many factors have influences on the evaluation of the cooling strategy like cost, weight, space, pump power and cooling performance [3].

In order to solve the two kinds of temperature problems mentioned above, some cooling measures can be arranged accordingly. For example, the heat generated by a battery can be taken away through fluid flow or energy storage materials to control the temperature of the battery. The surface of the battery can also be locally cooled to improve the temperature uniformity inside the battery. According to heat dissipation mechanism, main types of cooling strategies for battery thermal management (BTM) are classified as air cooling, heat pipe cooling, phase change material (PCM), liquid cooling and their combination [4, 5].

Air cooling is simple and cheap, and it was the first and common cooling technology applied in battery thermal management [6–9]. But it was limited owing to its low specific heat which led to rapid temperature rise along the air flow and low thermal conductivity which caused poor convective heat transfer coefficient especially when the required battery capacity was large or the ambient temperature was high. Heat pipe cooling is compact and doesn't need extra power supply in battery thermal management [10–13]. But a suitable condensing volume in battery compartment is a challenge topic. PCM cooling is also a passive cooling method that can absorb the heat generated by the battery and keeps battery temperature in constant because of the phase change [14–17]. The biggest problem of PCM cooling system is the poor ability to adjust cooling capacity to adopt different kinds of weather and thermal situations, and may work inefficiently after its completely melting.

Liquid cooling for BTM has been the most promising and popular cooling method for its good cooling capacity and easy adjustment control by changing the pump power [18–28]. The liquid cooling is divided into two different kinds generally. One is indirect, and employs tube, cooling plate and so on to prevent the liquid from contacting the battery [22–24]. The heat generated by batteries is transferred by the convection or flow boiling of liquid. The other is direct, and the batteries are immersed in the liquid [25, 26]. The heat generated by batteries is transferred from the battery to the liquid by the form of convection or pool boiling. There are many aspects worth of being researched in liquid cooling such

as the different kinds of liquid, single-phase heat transfer or two-phase heat transfer, different designs of the cooling plate or tube, and so on.

There were kinds of structures for cooling channels used in the current research. According to the layout of the channel, it can be divided into: serpentine channel [18, 27], uniform multi-channel [19, 29], topological channel [30] and so on. An et al. [29] studied experimentally the multi-mini-channels cooling performance applying in the battery module thermal management, and the results indicated that it could control the maximum temperature and improve the temperature uniformity of the battery module efficiently. One of the disadvantages of uniform multi-channel cooling plate is that it does not match the non-uniform distribution of the generated heat by batteries. The cooling plate with gradient-variable mini-channels can solve this problem, and improve the uniformity of battery surface temperature.

Some coolants, like refrigerant [26], water [31], oil [1] and glycol [1] have been studied. The thermal properties, such as thermal conductivity and specific heat, should be considered to choose as the coolant of the liquid cooling. The specific heat and thermal conductivity of deionized water are high compared to the other coolant, so it's often used for single-phase experiment. Flow boiling heat transfer is an efficient heat dissipation way. Selecting a coolant whose boiling point is within the optimal operating temperature range of the battery can achieve efficient battery thermal management effect with a low flow rate.

For different types of lithium-ion batteries, such as cylindrical battery, prismatic battery and pouch battery, different designs of battery tabs arrangement, different scales and different module structures assembled by the single cells, the thermal management methods and design parameters need to be specifically designed and optimized. Excellent battery thermal management system needs to be comprehensive in terms of space, weight, cost (initial cost, running cost, maintenance cost), life, stability and reliability, etc.

In most studies, the battery thermal managements were based on the assumption of uniform and constant heat generation of batteries in discharge process. It does not match the actual heat generation characteristic of batteries. An et al. [32] established a one-dimensional electrochemical-thermal coupling model of a prismatic cell and found that non-uniform distribution of heat generation in the cell increased with the discharge rate. Du et al. [33] established a three-dimensional thermal simulation model and found that the heat generation of different part of the battery was different. Therefore, the feature of non-uniformity heat generation performed in Li-ion batteries should be considered in the design of battery thermal management. It will improve heat dissipation capacity and work efficiency.

In this study, an electrochemical thermal coupling model of lithium battery was established to study the heat generation characteristic. Two types of cooling plates were designed and optimized based on the analysis of simulation results. A large-capacity battery thermal management system with the mini-channels cooling plate was established. The effect of the structure of cooling plates on the cooling performance of BTM system was discussed with different discharge rates. A pouch lithium-ion battery was used as the test object and the maximum temperature and temperature difference on the surface were discussed at all test conditions.

2. Electrochemical Thermal Coupling Model of Lithium Battery

2.1 Coupling mechanism of the models

The battery used in this study is a pouch $Li_4Ti_5O_{12}$ power battery, whose parameters are presented in Table 1. The three-dimensional cell unit was divided into two different dimensions of models: one-dimensional isothermal electrochemical model and two-dimensional electrochemical-thermal coupled model. The models were established on the COMSOL Multiphysics 5.4 simulation platform.

Table 1 Parameters of the battery

Parameters	Numerical value
Nominal voltage/V	2.3
Capacity/Ah	40
Length/mm	200
Width/mm	160
Height/mm	11.3

As shown in Fig. 1, the one-dimensional isothermal electrochemical model was used to simulate the porous negative electrode, the separator and the porous positive electrode. The two-dimensional electrochemical thermal coupling model was used to simulate the negative current collector and the positive current collector. The two models were coupled in the following way: the average heat generation density obtained by the one-dimensional model was used as the heat source of the two-dimensional model, and the average temperature of the two-dimensional model was used as the input temperature of the one-dimensional model.

2.2 The heat generation

A one-dimensional isothermal electrochemical model was established to calculate the heat generation in the porous electrodes and separator. Heat generation included reversible heat and irreversible heat. Irreversible heat

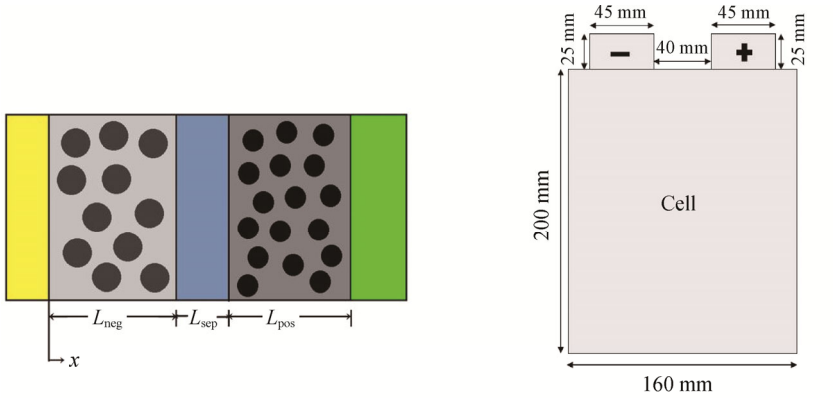

(a) One-dimensional electrochemical model (b) Two-dimensional electrochemical thermal coupling model

Fig. 1 Schematic of the models

Table 2 Expressions for various types of heat generation

Types	Expressions for heat generation
Reaction heat	$Q_{rea} = S_{a,i} j_{loc} T \frac{\Delta S_i}{F} = S_{a,i} j_{loc} T \frac{dU_i}{dT}, i = \text{neg, pos}$
Active polarization heat	$Q_{act} = S_{a,i} j_{loc} \eta, i = \text{neg, pos}$
Free electron ohmic heat	$Q_{ohm1} = -i_s \cdot \nabla \varphi_s$
Ion ohmic heat	$Q_{ohm2} = -i_l \cdot \nabla \varphi_l$

Table 3 Governing equations of the electrochemical thermal coupling model

Physical process	Part	Governing equations
Electric charge conservation	Non-electrode tab	$-\sigma_{cc,i} \nabla^2 \varphi_{\pm} = \pm \frac{i_{app}}{\delta_{cc,i}}, i = \text{neg, pos}$
	Electrode tab	$\sigma_{cc,i} \nabla^2 \varphi_{\pm} = 0, i = \text{neg, pos}$

included active polarization heat and ohmic heat. Ohmic heat could be further divided into ion ohmic heat and free electron ohmic heat. The specific expressions for different types of heat generation are shown in Table 2.

The heat generation in the porous negative electrode and porous positive electrode included reaction heat, active polarization heat, free electron ohmic heat and ion ohmic heat, given as follows:

$$Q_{total} = Q_{rea} + Q_{act} + Q_{ohm1} + Q_{ohm2} \quad (1)$$

The heat generation in the porous separator only came from ion ohmic heat and expressed as follows:

$$Q_{total} = Q_{ohm2} \quad (2)$$

As the heat generation distribution on the microscale (135 μm) was of little significance to the macroscopic heat dissipation, this model focused on the average heat generation density of the cell unit, which could be determined by the following equation:

$$Q_{ave} = \frac{\int_0^{L_{neg}+L_{sep}+L_{pos}} Q_{total} dx}{L_{neg} + L_{sep} + L_{pos}} \quad (3)$$

The influences of current collectors on the heat generation were the accumulation and dispersion of current during discharge process, which caused the non-uniformity of the battery's heat generation. The current collector was divided into electrode tab part and non-electrode tab part. The governing equations are shown in Table 3.

After getting the potential distribution of positive and negative current collector, the ohmic heat generation distribution of collectors could be calculated by the following equations:

$$i_{X,i} = -\sigma_{cc,i} \frac{\partial \varphi_{cc}}{\partial X}, i_{Y,i} = -\sigma_{cc,i} \frac{\partial \varphi_{cc}}{\partial Y}, i = \text{neg, pos} \quad (4)$$

$$Q_{cc,i} = \frac{1}{\sigma_{cc,i}} \left(i_{X,i}^2 + i_{Y,i}^2 \right), i = \text{neg, pos} \quad (5)$$

2.3 Boundary and initial conditions

The solid phase potential at the left boundary is expressed as follows:

$$\varphi_s \big|_{x=0} = 0 \quad (6)$$

The equations of the solid phase current and liquid phase current at the boundary of the electrodes and separator are shown in follows, while the symbols "–"

and "+" refer to the left and right sides of the interface:

$$i_{\mathrm{s}}\big|_{x=L_{\mathrm{neg}}+L_{\mathrm{sep}}+L_{\mathrm{pos}}}=i_{\mathrm{app}} \tag{7}$$

$$i_{\mathrm{s}}\big|_{x=L_{\mathrm{neg}}}=i_{\mathrm{s}}\big|_{x=L_{\mathrm{neg}}+L_{\mathrm{sep}}}=0 \tag{8}$$

$$i_{\mathrm{l}}\big|_{x=0}=i_{\mathrm{l}}\big|_{x=L_{\mathrm{neg}}+L_{\mathrm{sep}}+L_{\mathrm{pos}}}=0 \tag{9}$$

$$i_{\mathrm{l}}\big|_{x=L_{\mathrm{neg}}-}=i_{\mathrm{l}}\big|_{x=L_{\mathrm{neg}}+} \tag{10}$$

$$i_{\mathrm{l}}\big|_{x=\left(L_{\mathrm{neg}}+L_{\mathrm{sep}}\right)-}=i_{\mathrm{l}}\big|_{x=\left(L_{\mathrm{neg}}+L_{\mathrm{sep}}\right)+} \tag{11}$$

The lithium ion fluxes at the left boundary of the porous negative and the right boundary of the porous positive were zero. The lithium ion fluxes were continuous at the interface between the porous electrodes and the separator. The equations are shown in follows:

$$N_{\mathrm{l}}\big|_{x=0}=N_{\mathrm{l}}\big|_{x=L_{\mathrm{neg}}+L_{\mathrm{sep}}+L_{\mathrm{pos}}}=0 \tag{12}$$

$$N_{\mathrm{l}}\big|_{x=L_{\mathrm{neg}}-}=N_{\mathrm{l}}\big|_{x=L_{\mathrm{neg}}+} \tag{13}$$

$$N_{\mathrm{l}}\big|_{x=\left(L_{\mathrm{neg}}+L_{\mathrm{sep}}\right)-}=N_{\mathrm{l}}\big|_{x=\left(L_{\mathrm{neg}}+L_{\mathrm{sep}}\right)+} \tag{14}$$

In the one-dimensional electrochemical model, the dependent variables were solid phase potential, liquid phase potential and lithium ion concentration. There were 8 initial conditions as shown in Table 4.

Table 4 Initial conditions of the model

Area	Initial conditions
Porous negative electrode	$\varphi_{\mathrm{s}}=0,\varphi_{\mathrm{l}}=-U_{\mathrm{neg}},c_{\mathrm{l}}=c_{\mathrm{l},0}$
Porous separator	$\varphi_{\mathrm{l}}=-U_{\mathrm{neg}},c_{\mathrm{l}}=c_{\mathrm{l},0}$
Porous positive electrode	$\varphi_{\mathrm{s}}=U_{\mathrm{pos}}-U_{\mathrm{neg}},\varphi_{\mathrm{l}}=-U_{\mathrm{neg}},c_{\mathrm{l}}=c_{\mathrm{l},0}$

3. Experiments

3.1 Experimental apparatus

The schematic diagram of the cooling circulation system is illustrated in Fig. 2. The coolant driven from the reservoir flowed across the preheater which was used to adjust the cooling plate inlet temperature of coolant by changing the heating power. The coolant flowed through the cooling plate with mini-channels and cooled down the battery. The coolant would be cooled down by a plate heat exchanger. A Coriolis-type mass flow meter (SIEMENS SITRANS FC MASS 6000) was installed after the plate heat exchanger to measure the mass flow rate. Three pairs of temperature transmitters and pressure sensors were arranged before the mini-channels cooling plate, after the mini-channels cooling plate and the plate heat exchanger. The charge and discharge of pouch battery were controlled by a battery test station (Neware BTS-60V100A).

Deionized water and R141b were chosen as the coolants in this paper. The R141b is a kind of dielectric liquid in case the liquid leakage, and is stable at high temperature, non-flammable in case the battery catches fire. Another factor is that the boiling temperature of the R141b is 32°C at room pressure respectively, which is located in the optimal operating temperature range for the battery, 25°C–40°C. Deionized water was used for single-phase experiment. The thermal properties of coolants at 25°C are listed in Table 5.

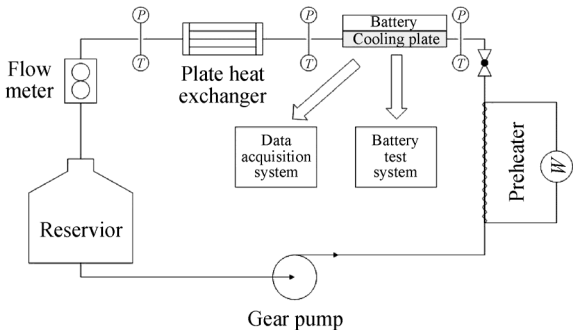

Fig. 2 Schematic diagram of the cooling system

Table 5 Thermal properties of the coolants

	Water	R141b
Density/kg·m^{-3}	997	1234
Specific heat/J·kg^{-1}·K^{-1}	4181	1154
Thermal conductivity/W·m^{-1}·K^{-1}	0.607	0.091
Boiling point at room pressure/°C	–	32.05
Latent heat of vaporization/kJ·kg^{-1}	–	223

3.2 Thermocouples distribution

As shown in Fig. 3, eleven T-type thermocouples were arranged to monitor the temperature during the discharge process. The measuring points 1 and 2 were symmetrically arranged 20 cm directly below the two electrode tabs. Point 3 was arranged in the center of the battery surface. Point 4 and point 5 were arranged symmetrically, and the horizontal and vertical distance from point 4 to the bottom left of the battery was 20 cm. There were six points arranged symmetrically on surface of the cooling plate. The temperature data were collected by an Agilent 34970A Data Acquisition.

3.3 Uncertainty analysis

Temperature data of the battery surface were measured by five T-type thermocouples. The temperatures and pressures of the coolant at inlet and outlet of the cooling plates and after the plate heat exchanger were measured by temperature transmitter and pressure sensor, respectively. The current and voltage of the battery were acquired by the battery test station. The mass flow rate was measured by the mass flow meter. The accuracy of main devices is summarized in Table 6.

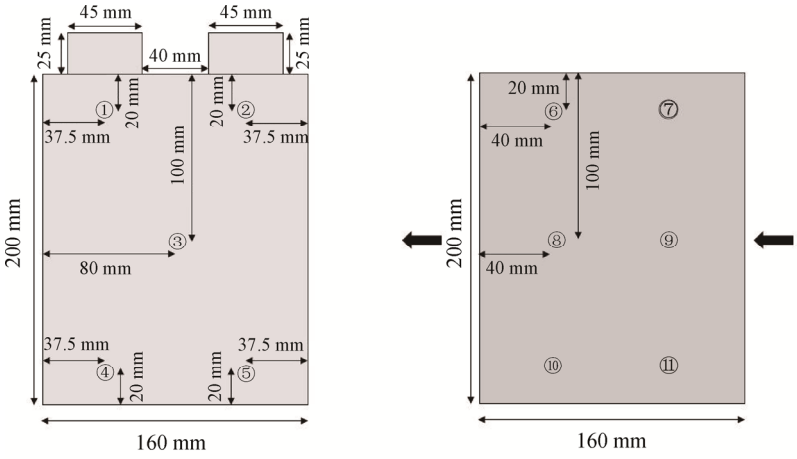

(a) Thermocouples on battery (b) Thermocouples on cooling plate

Fig. 3 Distribution of the thermocouples

Table 6 Accuracy of the data

Parameters	Uncertainty
Temperature transmitter	±0.1°C
Pressure transmitter	±0.4%
P, pressure sensor	±1%
q, mass flow meter	±2%
Q, heat power	±2.4%

4. Results and Discussion

4.1 Heat generation characteristic of pouch lithium battery

The battery heat generation densities with 1C, 2C and 2.5C discharge rates are presented in Fig. 4. It was indicated that the heat generation density of the battery increased with the process of discharge. In the initial period, the heat generation density increased rapidly due to the increase of reaction heat. The heat generation density with 2.5C discharge rate was about 20 000 W/m^3, which was 1.69 times and 3.67 times of that with 2C discharge rate and 1C discharge rate. At the later stage of discharge, since the intensification of polarization caused the polarization heat rapidly increased, the heat generation density sharply increased again. The heat generation density with 2.5C discharge rate was 40 000 W/m^3, which was 1.29 times of that with 2C discharge rate and 1.82 times of that with 1C discharge rate. The simulation results indicated that more attention should be paid to the heat dissipation of the battery with high discharge rate. With 2.5C discharge rate, the heat generation density at the end of discharge was 1.82 times of that at the beginning of discharge. Therefore, for the battery cooling strategy, it is more important to strengthen the heat dissipation in the later period of battery discharge.

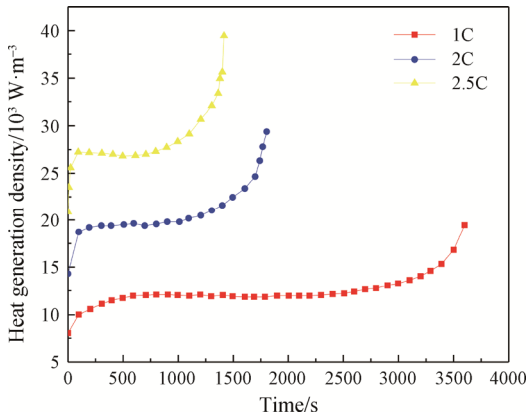

Fig. 4 Battery heat generation density with 1C, 2C and 2.5C discharge rates

As the battery was discharged with constant current, the heat generation density at a specific area on current collectors was constant. However, the heat generation density at different areas on the collector was not uniform. Fig. 5 shows the ohmic heat generation distribution on the current collectors with 2.5C discharge rate. The heat generation of positive current collector was about 1.5 times as much as that of the negative current collector. Besides, since there was only ohmic heat on the current collectors, the non-uniformity of heat generation distribution increased with the discharge rate.

The total heat generation of battery was the sum of heat generation calculated by one-dimensional model and two-dimensional model. The distributions of total heat generation at the beginning, middle and end of discharge are shown in Fig. 6. The heat generation density was higher in the area near the electrode tab due to the concentration of current. The temperature in the area near the electrode tab was higher. The main reason was that the heat generation density was higher and the electrode tab conducted joule heat generation.

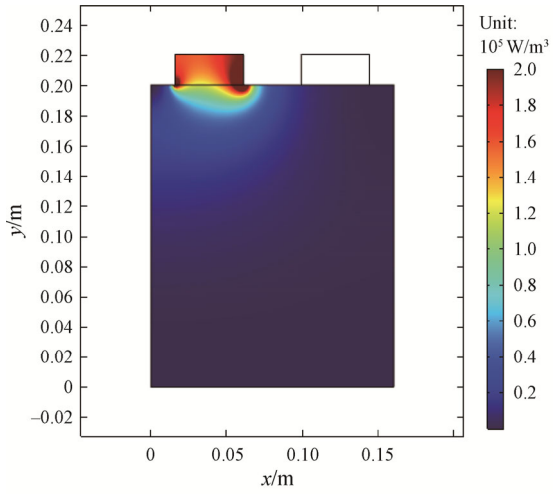

(a) Negative current collector

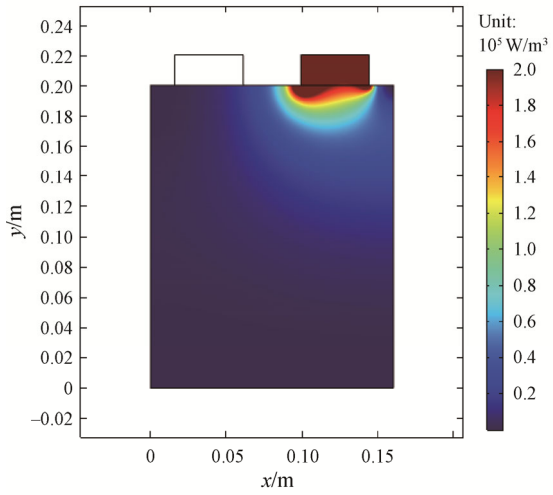

(b) Positive current collector

Fig. 5 Heat generation density distribution of negative and positive current collector

Since the heat generation of current collectors was seriously non-uniform, the heat generation characteristic of the battery calculated by the above model could be used as a guide for the cooling strategy, which was also the basis of designing the non-uniform structure mini-channels cooling plate to improve the heat dissipation.

4.2 Design of mini-channels cooling plate

The design of cooling plate should match with the heat generation characteristic of battery. For analyzing the distributions of heat generation, the current collectors were evenly divided into 10 parts according to the distance from electrode tabs. The heat generation density of different parts of each current collector with 2.5C discharge rate is shown in Table 7. It was indicated that 46% of the total ohmic heat was generated in the tenth part. This was the main reason for the non-uniform temperature distribution of the battery.

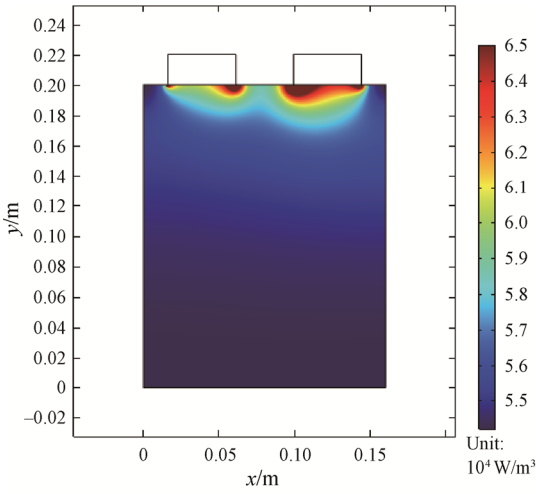

(a) The distribution of total heat generation at the beginning of discharge

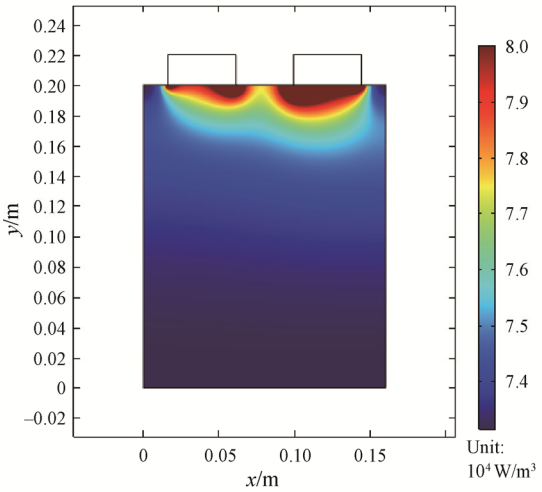

(b) The distribution of total heat generation at the middle of discharge

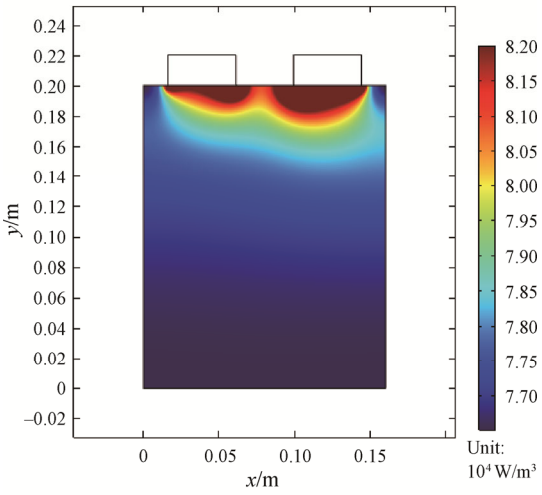

(c) The distribution of total heat generation at the end of discharge

Fig. 6 Distribution and variation of total heat generation density

Table 7 Heat generation density of different parts of current collectors with 2.5C discharge rate

Part	Heat generation density of negative current collector/W·m^{-3}	Heat generation density of positive current collector/W·m^{-3}	Total heat generation density/W·m^{-3}	Proportion
1	37.526	59.640	97.166	<0.1%
2	197.38	313.69	511.07	<1%
3	522.22	829.96	1352.18	1%
4	1025.7	1630.1	2655.8	2%
5	1738.8	2763.4	4502.2	3%
6	2730.0	4338.7	7068.7	5%
7	4151.5	6597.9	10 749.4	8%
8	6354.4	10 099	16 453.4	13%
9	10 338	16 431	26 769	21%
10	22 688	36 058	58 746	46%
Electrode tab	98 190	156 050	–	5%

Based on the heat generation characteristic of the battery, a cooling plate with variable mini-channels was designed in this study. The wider channel was arranged closer to the electrode tab to improve the heat dissipation. There were 3 channels with 5 mm in width and 1 mm in height, 2 channels with 4 mm in width and 1 mm in height, 6 channels with 3 mm in width and 1 mm in height, 2 channels with 2 mm in width and 1 mm in height, and 3 channels with 1 mm in width and 1 mm in height. A cooling plate with 16 channels uniformly arranged was designed as a compared experiment. The channel was 3 mm in width and 1 mm in height. The arrangement of the channels is shown in Fig. 7. Although the structure of the two cooling plates was different, the total cross-sectional area, total heat transfer area and total mass flow rate were the same. The material of cooling plate was copper.

4.3 Single-phase cooling with deionized water

Deionized water was used in the single-phase cooling experiment for its high specific heat and thermal conductivity. As shown in Fig. 8, the cooling plate with variable mini-channels had a lower maximum temperature and better temperature distribution uniformity on battery surface with 2.5C discharge rate. The maximum temperature for the cooling plate with uniform mini-channels was 39.4°C at the end of discharge process, while the maximum temperature for the cooling plate with variable mini-channels was 37.1°C. The temperature of point 1 was higher than that of point 2 in the discharge process, which was consistent with the simulation results that the heat generation of positive current collector was higher than that of the negative current collector.

By comparing the cooling performance of the two cooling plates, the temperature at the point near the electrode tabs of the cooling plate with variable mini-channels was lower than that of the cooling plate with uniform mini-channels. The temperature at the points away from the electrode tabs of the cooling plate with the variable mini-channels was higher than that of the cooling plate with the uniform mini-channels. The temperature of point 4 at the end of discharge was 32.7°C for the cooling plate with variable mini-channels, and that was 31.1°C for the cooling plate with uniform mini-channels. The cooling plate with variable mini-channels could match the non-uniformity heat generation from the battery. Because the cross sections of the channels near the electrode tabs were larger than those away from the electrode tabs, more coolant mass could flow near the electrode tabs. The design of this structure improved the cooling capacity of the cooling plate.

As shown in Fig. 9, the maximum temperature difference through the discharge process for the cooling plate with uniform mini-channels was 10.7°C, while that for the cooling plate with variable mini-channels was 6.2°C. Therefore, the latter had better cooling performance. The temperature difference increased quickly at the beginning of discharge process, and became lower when the discharge was close to the end.

Since phase change did not occur in the single-phase cooling, the heat absorption could be calculated by the temperature at the inlet and outlet and the mass flow rate of the deionized water. As shown in Fig. 10, the heat absorption by the two types of cooling plate in the discharge process was approximately the same. Because the total heat transfer area of the 16 channels was the same and the mass flow was the same in the two cooling plates. The advantage of the cooling plate with variable mini-channels was that it absorbed more heat generation near the electrode tabs and improved the temperature uniformity of the battery.

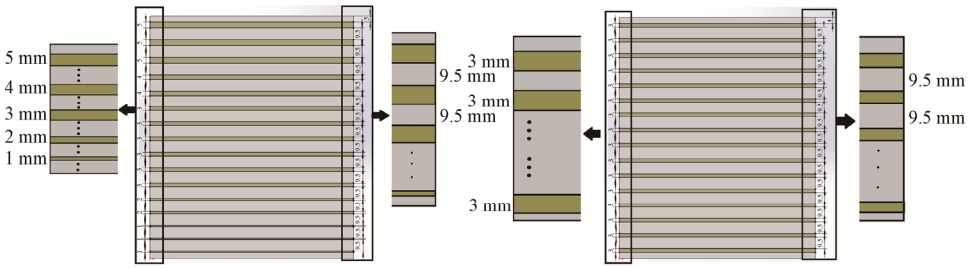

(a) The cooling plate with variable mini-channels (b) The cooling plate with uniform mini-channels

Fig. 7 Schematic of arrangement of channels in the mini-channels cooling plates

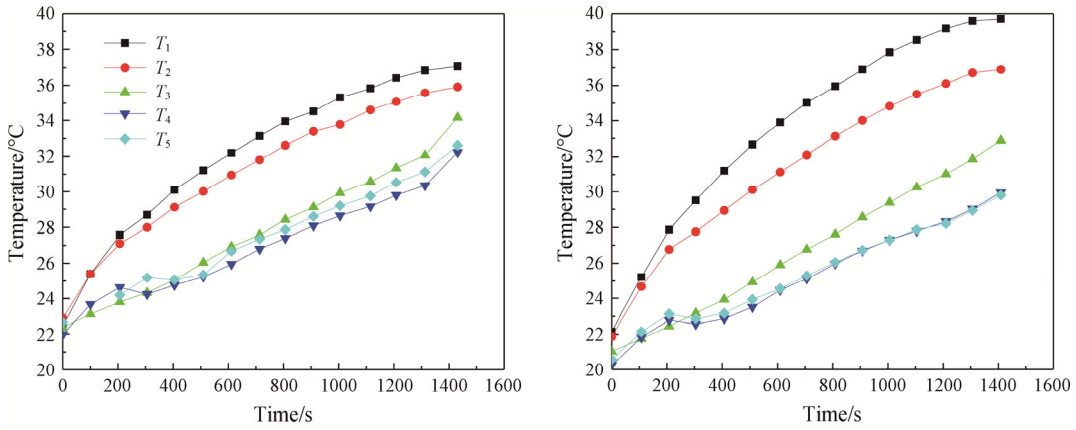

(a) The cooling plate with variable mini-channels (b) The cooling plate with uniform mini-channels

Fig. 8 Temperature distribution of the battery with 2.5C discharge rate (water cooling)

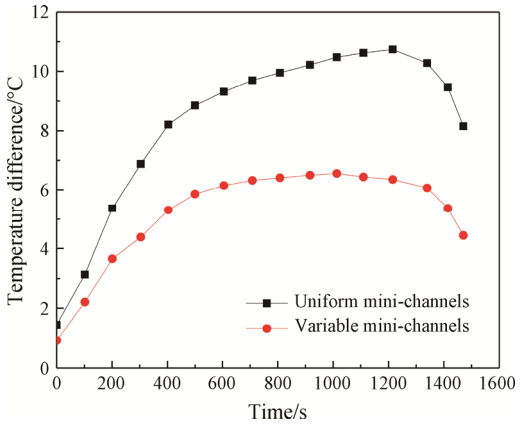

Fig. 9 Temperature difference on the cooling plates in the discharge process with 2.5C discharge rate

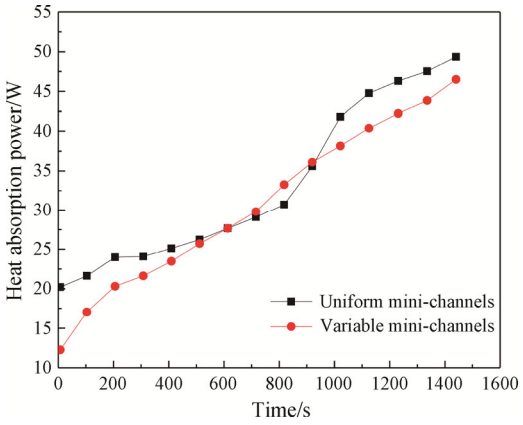

Fig. 10 Heat absorption by the coolant

Fig. 11 shows the temperature distribution of battery surface in the process with 2C discharge rate. The maximum temperature on the battery surface arrived up to 33.5°C at the end of the discharge process for the cooling plate with variable mini-channels, while 36.2°C for the cooling plate with uniform mini-channels. The cooling plate with variable mini-channels had a better temperature distribution than the cooling plate with uniform mini-channels. The maximum temperature difference was 4.3°C for the cooling plate with variable mini-channels, while 8.0°C for the cooling plate with uniform mini-channels. For lower heat generation in 2C discharge rate, the maximum temperature difference (4.3°C) is lower than it for 2C discharge rate (6.2°C) with variable mini-channels.

As shown in Fig. 12, the maximum temperature of battery surface was 30.0°C at the end of 1.5C discharge process for the cooling plate with variable mini-channels, while 31.6°C for the cooling plate with uniform mini-channels. The maximum temperature was located at

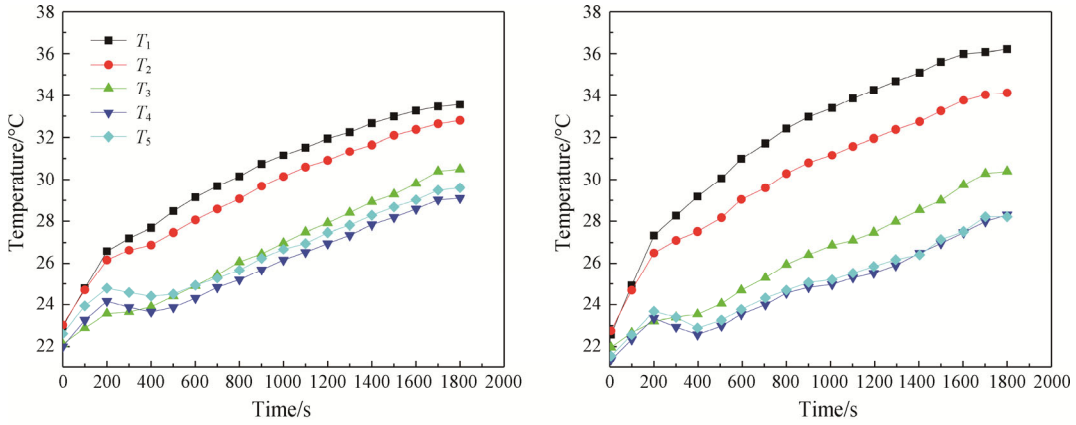

(a) The cooling plate with variable mini-channels (b) The cooling plate with uniform mini-channels

Fig. 11 Temperature distribution of the battery with 2C discharge rate (water cooling)

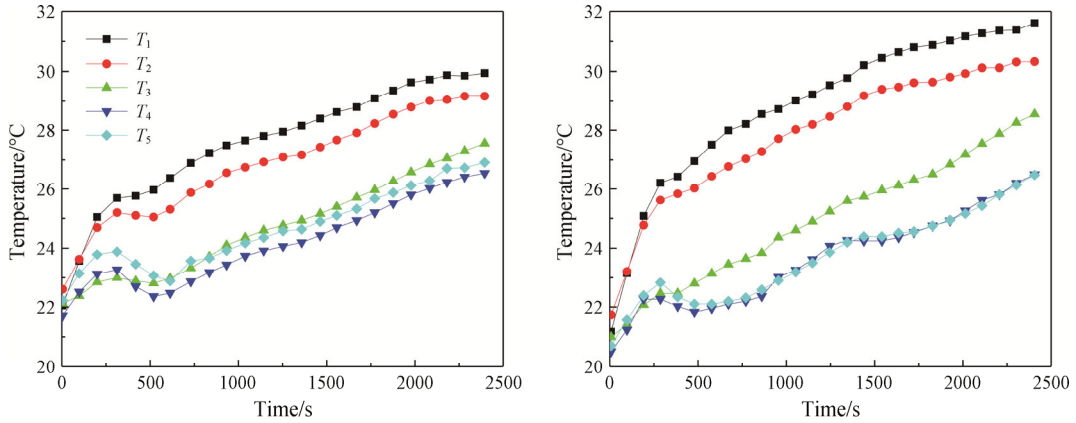

(a) The cooling plate with variable mini-channels (b) The cooling plate with uniform mini-channels

Fig. 12 Temperature distribution of the battery with 1.5C discharge rate (water cooling)

point 1 in Fig. 3. The maximum temperature differences at the end of discharge process for the variable mini-channels cooling plate and uniform mini-channels cooling plate were 3.5°C and 5.1°C.

Compared with the cooling plate with uniform mini-channels, with 1.5C, 2C and 2.5C discharge rates, the maximum surface temperature decreased by 1.6°C, 2.7°C and 2.3°C and the maximum temperature difference decreased by 1.6°C, 3.7°C and 4.5°C. This proved that the cooling plate with variable mini-channels had better cooling effect and the effect on temperature uniformity increased with the discharge rate.

4.4 Two-phase cooling with refrigerant R141b

Because of the electroconductivity of deionized water, its practical application was limited. An insulating coolant was needed in the thermal management of batteries. Refrigerant R141b was selected as the coolant for the two-phase cooling experiment. With 2.5C discharge rate, the temperature distributions of the battery for the two types of cooling plate are shown in Fig. 13. The maximum temperature for the cooling plate with the uniform mini-channels at the end of discharge process was 45.6°C, while that for the cooling plate with variable mini-channels at the end of discharge process was 44.4°C. The maximum temperature difference on the surface of the battery through the discharge process for the cooling plate with the uniform mini-channels was 9.0°C, while that for the cooling plate with the variable mini-channels was 7.5°C. It was indicated the cooling plate with variable mini-channels had better cooling effect in the two-phase cooling as well.

Fig. 14(a) showed the outlet temperature of the coolant and the surface temperature of the cooling plate with variable mini-channels with 2.5C discharge rate. It was indicated that the outlet temperature reached the saturation temperature at 600 s and the coolant had a phase transition in the channels. As shown in Fig. 14(b), compared with the other five measuring points, the temperature at point 6 and point 7 reached the phase change point faster. It was because of the higher heat generation density near the electrode tab. Flow boiling heat transfer firstly occurred in the channel near the electrode tab, and then occurred in the channel far away

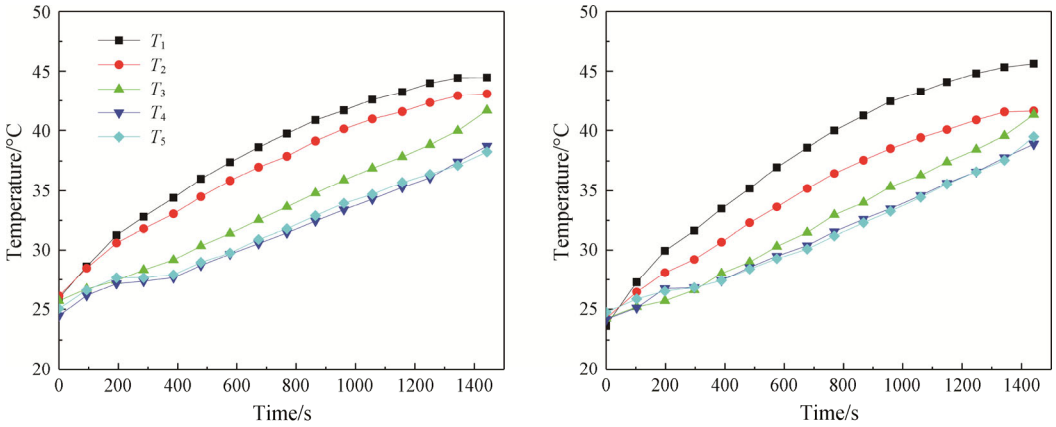

(a) The cooling plate with variable mini-channels (b) The cooling plate with uniform mini-channels

Fig. 13 Temperature distribution of the battery with 2.5C discharge rate (R141b cooling)

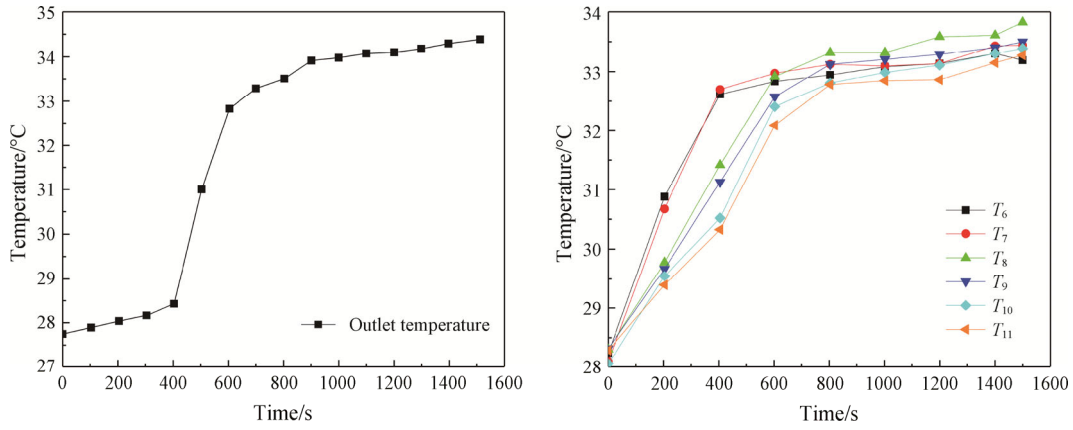

(a) Outlet temperature of the coolant (b) Surface temperature of the cooling plate

Fig. 14 Outlet temperature of the coolant and surface temperature of the cooling plate

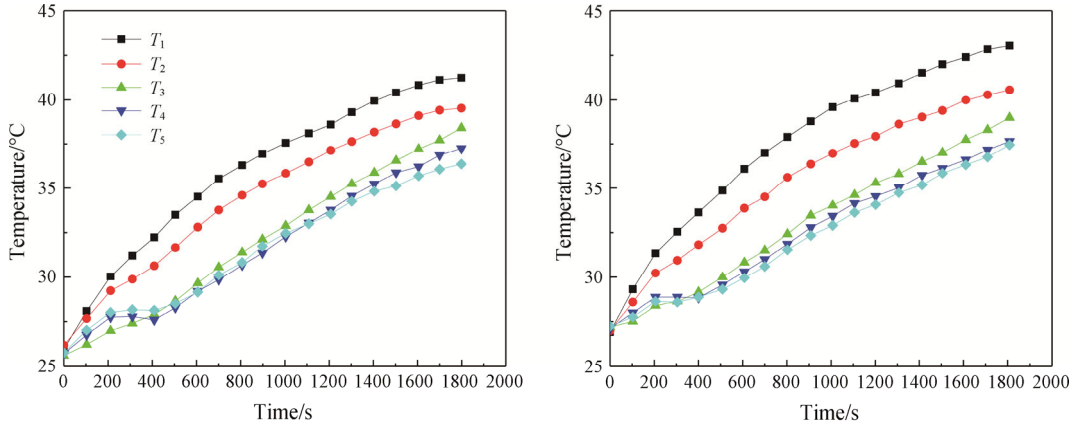

(a) The cooling plate with variable mini-channels (b) The cooling plate with uniform mini-channels

Fig. 15 Temperature distribution of the battery with 2C discharge rate (R141b cooling)

from the electrode tab. In the channels, flow boiling firstly occurred near the outlet due to the continuous absorption of heat by the coolant.

Fig. 15 shows the temperature distribution of battery surface in the process with 2C discharge rate. The maximum temperature on the battery surface arrived up to 41.3°C at the end of the discharge process for the cooling plate with variable mini-channels, while 43.2°C for the cooling plate with uniform mini-channels. The maximum temperature difference was 6.0°C for the cooling plate with variable mini-channels, while 6.8°C for the cooling plate with uniform mini-channels.

The results with 1.5C discharge rate with R141b cooling are shown in Fig. 16. It was indicated that the maximum temperature of the surface battery was 37.8°C at the end of discharge process for the cooling plate with variable mini-channels, while 39.5°C for the cooling plate with uniform mini-channels. The maximum temperature was located at point 1 in Fig. 3. The maximum temperature differences at the end of discharge process for the variable mini-channels cooling plate and uniform mini-channels cooling plate were 2.7°C and 5.4°C. With low discharge rate when the battery generated less heat, the cooling plate with variable mini-channels gave a better result for improving temperature uniformity. With 2C and 2.5C discharge rates, flow boiling occurred in the channels, and the effect of the cooling plate with variable mini-channels increased with the discharge rate.

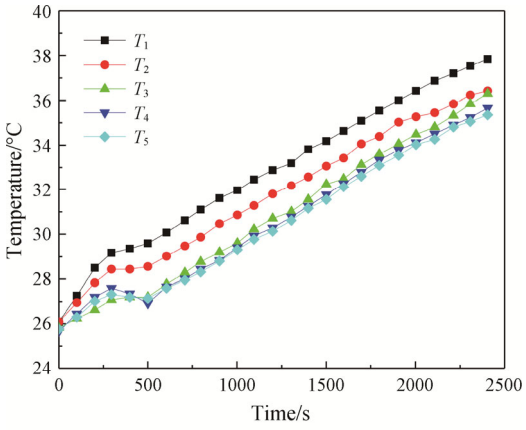

(a) The cooling plate with variable mini-channels

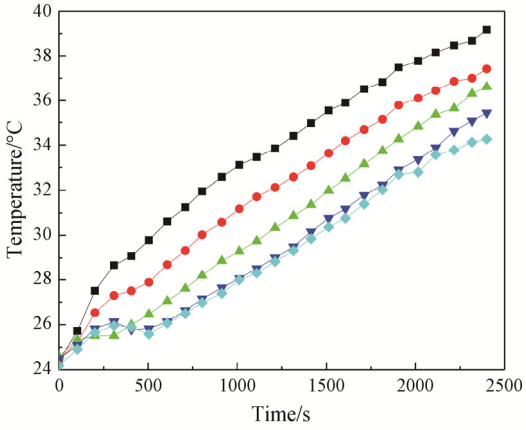

(b) The cooling plate with uniform mini-channels

Fig. 16 Temperature distribution of the battery with 1.5C discharge rate (R141b cooling)

5. Conclusions

In this paper, an electrochemical thermal coupling model of lithium battery was established to study the heat generation characteristic. Two mini-channels cooling plates (variable and uniform) were designed based on the heat generation characteristic. The cooling performance of the two cooling plates was compared. The main conclusions were summarized as follows:

(1) The heat generation density of battery increased with the discharge rate. At the beginning of the discharge, the heat generation density with 2.5C discharge rate was 1.69 times and 3.67 times of that with 2C discharge rate and 1C discharge rate. At the end of the discharge, the heat generation density with 2.5C discharge rate was 1.29 times of that with 2C discharge rate and 1.82 times of that with 1C discharge rate.

(2) The heat generation density of battery increased with the process of discharge. With 2.5C discharge rate, the heat generation density at the end of discharge was 1.82 times of that at the beginning of discharge.

(3) The heat generation density at different areas of the battery was not uniform. The simulation results showed that 46% of the total ohmic heat was generated near the electrode tabs. With 2.5C discharge rate, the heat generation of positive current collector was about 1.5 times as much as that of the negative current collector.

(4) A cooling plate with variable mini-channels designed based on heat generation characteristic of the battery showed a better cooling performance in both cooling experiments. The effect of the cooling plate with variable mini-channels increased with the discharge rate in high discharge rate cases. In the single-phase cooling with deionized water, compared with the cooling plate with uniform mini-channels, the maximum temperature difference decreased by 1.6°C, 3.7°C and 4.5°C with 1.5C, 2C and 2.5C discharge rates. In the two-phase cooling with refrigerant R141b, the maximum temperature difference decreased by 0.8°C and 1.5°C with 2C and 2.5C discharge rates.

Acknowledgements

This work was supported by the National Key R&D Program of China (2019YFE0104900).

References

[1] Pesaran A., Battery thermal management in EVs and HEVs: issues and solutions. Advanced Automotive Battery Conference, Las Vegas, Nevada, USA, 2001.

[2] Lu L., Han X., Li J., Hua J., Ouyang M., A review on the key issues for lithium-ion battery management in electric vehicles. Journal of Power Sources, 2013, 226: 272–288.

[3] Rao Z., Wang S., A review of power battery thermal energy management. Renewable and Sustainable Energy Reviews, 2011, 15: 4554–4571.

[4] Zhao R., Zhang S., Liu J., Gu J., A review of thermal performance improving methods of lithium ion battery: electrode modification and thermal management system. Journal of Power Sources, 2015, 299: 557–577.

[5] An Z., Jia L., Ding Y., Dang C., Li X., A review on lithium-ion power battery thermal management technologies and thermal safety. Journal of Thermal Science, 2017, 26(5): 391–412.

[6] Mahamud R., Park C., Reciprocating air flow for Li-ion battery thermal management to improve temperature uniformity. Journal of Power Sources, 2011, 196: 5685–5696.

[7] Wang T., Tseng K.J., Zhao J., Wei Z., Thermal investigation of lithium-ion battery module with different cell arrangement structures and forced air-cooling strategies. Applied Energy, 2014, 134: 229–238.

[8] Fan Y., Bao Y., Ling C., Chu Y., Tan X., Yang S., Experimental study on the thermal management performance of air cooling for high energy density cylindrical lithium-ion batteries. Applied Thermal Engineering, 2019, 155: 96–109.

[9] Pan S., Ji C., Wang S., Wang B., Study on the performance of parallel air-cooled structure and optimized design for lithium-ion battery module. Fire Technology, 2020, 56: 2623–2647.

[10] Putra N., Ariantara B., Pamungkas R.A., Experimental investigation on performance of lithium-ion battery thermal management system using flat plate loop heat pipe for electric vehicle application. Applied Thermal Engineering, 2016, 99: 784–789.

[11] Greco A., Cao D., Jiang X., Yang H., A theoretical and computational study of lithium-ion battery thermal management for electric vehicles using heat pipes. Journal of Power Sources, 2014, 257: 344–355.

[12] Ye Y., Saw L.H., Shi Y., Tay A.A.O., Numerical analyses on optimizing a heat pipe thermal management system for lithium-ion batteries during fast charging. Applied Thermal Engineering, 2015, 86: 281–291.

[13] Wang Q., Jiang B., Xue Q., Sun H., Li B., Zou H., Yan Y., Experimental investigation on EV battery cooling and heating by heat pipes. Applied Thermal Engineering, 2015, 88: 54–60.

[14] Javani N., Dincer I., Naterer G.F., Yilbas B.S., Heat transfer and thermal management with PCMs in a Li-ion battery cell for electric vehicles. International Journal of Heat and Mass Transfer, 2014, 72: 690–703.

[15] Huang Q., Li X., Zhang G., Deng J., Wang C., Thermal management of Lithium-ion battery pack through the application of flexible form-stable composite phase change materials. Applied Thermal Engineering, 2020, 183: 116151.

[16] Zhang J., Li X., Zhang G., Wu H., Rao Z., Guo J., Zhou D., Experimental investigation of the flame retardant and form-stable composite phase change materials for a power battery thermal management system. Journal of Power Sources, 2020, 480: 229116.

[17] Greco A., Jiang X., Cao D., An investigation of lithium-ion battery thermal management using paraffin/porous-graphite-matrix composite. Journal of Power Sources, 2015, 278: 50–68.

[18] Deng T., Zhang G., Ran Y., Study on thermal management of rectangular Li-ion battery with serpentine-channel cold plate. International Journal of Heat and Mass Transfer, 2018, 125: 143–152.

[19] Huo Y., Rao Z., Liu X., Zhao J., Investigation of power battery thermal management by using mini-channel cold plate. Energy Conversion and Management, 2015, 89: 387–395.

[20] Zhao J., Rao Z., Li Y., Thermal performance of mini-channel liquid cooled cylinder based battery thermal management for cylindrical lithium-ion power battery. Energy Conversion and Management, 2015, 103: 157–165.

[21] Rao Z., Wang Q., Huang C., Investigation of the thermal performance of phase change material/mini-channel coupled battery thermal management system. Applied Energy, 2016, 164: 659–669.

[22] Jin L.W., Lee P.S., Kong X.X., Fan Y., Chou S.K., Ultra-thin mini-channels LCP for EV battery thermal management. Applied Energy, 2014, 113: 1786–1794.

[23] Wei L., Jia L., An Z., Dang C., Experimental study on thermal management of cylindrical Li-ion battery with flexible microchannel plates. Journal of Thermal Science, 2020, 29(4): 1001–1009.

[24] Fang Y., Shen J., Zhu Y., Ye F., Li K., Su L., Investigation on the transient thermal performance of a mini-channel cold plate for battery thermal management. Journal of Thermal Science, 2021, 30: 914–925.

[25] Wang Y., Wu J., Thermal performance predictions for an HFE-7000 direct flow boiling cooled battery thermal management system for electric vehicles. Energy Conversion and Management, 2020, 207: 112569.

[26] Bandhauer T.M., Garimella S., Passive, Internal thermal management system for batteries using microscale liquid-vapor phase change. Applied Thermal Engineering, 2013, 61(2): 756–769.

[27] Sheng L., Su L., Zhang H., Li K., Fang Y., Ye W., Fang Y., Numerical investigation on a lithium ion battery thermal management utilizing a serpentine-channel liquid cooling plate exchanger. International Journal of Heat and Mass Transfer, 2019, 141: 658–668.

[28] Monika K., Chakraborty C., Roy S., Dinda S., Singh S.A., Datta S.P., An improved mini-channel based liquid cooling strategy of prismatic $LiFePO_4$ batteries for

electric or hybrid vehicles. Journal of Energy Storage, 2021, 35: 102301.

[29] An Z., Jia L., Li X., Ding Y., Experimental investigation on lithium-ion battery thermal management based on flow boiling in mini-channel. Applied Thermal Engineering, 2017, 117: 534–543.

[30] Ju X., Xu C., Zhou Y., Liao Z., Yang Y., Numerical investigation of a novel manifold micro-pin-fin heat sink combining chessboard nozzle-jet concept for ultra-high heat flux removal. International Journal of Heat and Mass Transfer, 2018, 126: 1206–1218.

[31] Panchal S., Dincer I., Agelin-Chaab M., Fraser R., Fowler M., Experimental and theoretical investigation of temperature distributions in a prismatic lithium-ion battery. International Journal of Thermal Sciences, 2016, 99: 204–212.

[32] An Z., Jia L., Wei L., Dang C., Peng Q., Investigation on lithium-ion battery electrochemical and thermal characteristic based on electrochemical-thermal coupled model. Applied Thermal Engineering, 2018, 137: 792–807.

[33] Du S., Jia M., Cheng Y., Tang Y., Zhang H., Ai L., Zhang K., Lai Y., Study on the thermal behaviors of power lithium iron phosphate (LFP) aluminum-laminated battery with different tab configurations. International Journal of Thermal Sciences, 2015, 89: 327–336.